Materials Science & Engineering A 760 (2019) 407–414

Contents lists available at ScienceDirect

Materials Science & Engineering A

journal homepage: www.elsevier.com/locate/msea

The gradual disappearance of yield plateau in Zr–Sn–Nb–Fe–Mo alloy by the trace addition of Cr and V

Huigang Shi[a], Xianglong Guo[b], Jiuxiao Li[c,**], Jianwei Mao[a], Weijie Lu[a,*]

[a] State Key Laboratory of Metal Matrix Composites, School of Material Science and Engineering, Shanghai Jiao Tong University, Shanghai, 200240, China
[b] School of Nuclear Science and Engineering, Shanghai Jiao Tong University, NO. 800 Dongchuan Road, Shanghai, 200240, China
[c] School of Materials Engineering, Shanghai University of Engineering Science, Shanghai, 201620, China

ARTICLE INFO

Keywords:
Zirconium alloy
Tensile properties
Yield plateau
Microstructure
Re-crystallization
Dislocation density

ABSTRACT

Trace chromium (Cr, 0.1 wt. %) and vanadium (V, 0.05 wt. %) were doped to the Zr–Sn–Nb–Fe–Mo alloy (denoted as Zir) to investigate the tensile properties at room temperature. A clear yield plateau was observed in Zir alloy, while the yield plateau was gradually disappeared by the addition of Cr to Zir alloy (denoted as Zir-0.1Cr) and by the combined addition of Cr and V to Zir alloy (denoted as Zir-0.1Cr-0.05 V). Microscopic characterization results revealed that doping of Cr and V retarded the re-crystallization process in Zir alloy. Firstly, the mean grain size of matrix was reduced from 1.9 μm to 1.7 μm and 1.5 μm by addition of 0.1% Cr and 0.1% Cr + 0.05% V to Zir alloy, respectively. The fraction of low angle grain boundaries (LAGBs) increased from 50.2% to 53.9% and 60.8% in Zir-0.1Cr and Zir-0.1Cr-0.05 V, respectively. Secondly, the volume fraction of second phase particles (SPPs) increased from 7.2% to 11.1% and 11.8% in Cr-containing and Cr + V-containing alloys, respectively. The mechanism of yield plateau in our alloy was explained by the impurity-dislocation interaction and dislocation multiplication mechanism, and the gradual disappearance of yield plateau behavior at the early stage of yielding could be attributed to the gradual increment of mobile dislocation density in Zir-0.1Cr and Zir-0.1Cr-0.05 V alloys. The tensile tests with different pre-strains proved that the gradual disappearance of yield plateau was caused by the increase of mobile dislocations with increasing pre-strain.

1. Introduction

Zirconium alloys have long been used in nuclear reactors because of their high corrosion resistance, appropriate mechanical properties, and low thermal neutron absorption cross-section [1,2]. Mechanical properties of zirconium alloys are one of the main factors for the performance of zirconium alloy tubes operated at higher fuel burn-up and more fuel cycles [3–6]. It is well known that the mechanical properties can be improved by properly adjusting the chemical compositions, which can effectively optimize the microstructure of zirconium alloys. As a typical alloying element, Cr addition into Zr-based alloys has been investigated by many researchers. For instance, Yang [7] reported that the grain size was gradually decreased and the yield strength was gradually increased with the increment of Cr content in Zr-*x*Cr alloy. Jung [8] reported that the doping of Cr exhibited creep strengthening effect in Zr–Sn–Nb alloys. The effect of V addition has also been studied and it was found that the V addition can stabilize the C36 structure of the $ZrCr_2$ Laves phase [9].

The yield drop phenomenon has been widely reported in different alloys such as low carbon steels [10–12], Ti alloys [13–16], Al alloys [17] and Mg alloys [18,19]. In general, the mechanism accounting for the yield drop has been discussed on the basis of dislocation theories. In metallic alloys, it is assumed that the primary dislocations are not able to convey the initial stages of yielding, and the existence of solute atoms is considered to be one of the main factors, which can be attracted to the strain field surrounding immobilized dislocations to form Cottrell atmosphere [20]. Recently, we found that a new Zr-based alloy exhibited a yield plateau in the tension tests at room temperature. The yield plateau at the initial stage of plastic deformation, actually, can be seen as one of most common yield drop phenomena, with minor difference among the upper and lower yield points. The yield drop phenomenon in zirconium alloys has been investigated by some researchers [21–25]. For instance, Veevers [22] studied that the dislocation cell microstructure was the prerequisite for the yield drop to happen and

* Corresponding author State Key Laboratory of Metal Matrix Composites, School of Material Science and Engineering, Shanghai Jiao Tong University, Shanghai 200240, PR China.
** Corresponding author.School of Materials Engineering, Shanghai University of Engineering Science, Shanghai 201620, PR China.
E-mail addresses: lijiuxiao@126.com (J. Li), luweijie@sjtu.edu.cn (W. Lu).

https://doi.org/10.1016/j.msea.2019.06.023
Received 16 March 2019; Received in revised form 6 June 2019; Accepted 7 June 2019
Available online 08 June 2019
0921-5093/

Table 1
Chemical composition (in wt. %) of the materials studied in this work.

Alloy	Elements						
	Zr	Sn	Nb	Fe	Mo	Cr	V
Zir	Bal.	0.34	0.74	0.31	0.14	–	–
Zir-0.1Cr	Bal.	0.37	0.75	0.30	0.16	0.11	–
Zir-0.1Cr-0.05 V	Bal.	0.36	0.77	0.29	0.16	0.11	0.058

the locking of dislocations by oxygen interstitial atoms was responsible for the yield drop in Zircaloy-2. Thorpe [23] believed that the dislocation locking was caused by the stress-induced Snoek ordering mechanism [24], which was responsible for the yield drop in Zr–1Nb alloy. Ko [25] reported the yield stress plateau in the annealed Zr-1.5Nb alloy, which was caused by the interaction between oxygen/sulphur atoms and dislocations.

However, there is little study in regard to the effect of alloying elements Cr and V on the yield plateau behavior at the initial stage of plastic deformation, and the possible origin of this behavior is not clear. In this paper, a Zr–Sn–Nb–Fe–Mo alloy with a series of heat treatments was designed and a yield plateau during the tensile test was observed. The influences of trace Cr and V addition on this behavior were examined by microstructure characterization. This would provide new insights into the underlying mechanisms of yield plateau in metallic alloys.

2. Experimental procedures

2.1. Material preparation

Three zirconium alloys with nominal chemical compositions of Zr-0.35Sn-0.75Nb-0.3Fe-0.1Mo (denoted as Zir), Zr-0.35Sn-0.75Nb-0.3Fe-0.1Mo-0.1Cr (denoted as Zir-0.1Cr) and Zr-0.35Sn-0.75Nb-0.3Fe-0.1Mo-0.1Cr-0.05 V (denoted as Zir-0.1Cr-0.05 V) were prepared by a sequence of three vacuum arc re-melting to obtain the chemical homogeneity. The detailed chemical composition of the different alloys is shown in Table 1. The ingots were forged to 10 mm thick at 1273 K and then solution annealed at 1323 K for 30 min before water quenching. After that, a serial of hot rolling was conducted at 923 K to reduce the thickness of materials to 4.7 mm. Then the materials were cold rolled to 0.65 mm in thickness with three intermediate heat treatments at 823 K for 4 h. The final annealing treatment is 823 K for 5 h, and the sequence of heat treatments is illustrated in Fig. 1.

2.2. Microstructure characterization

The microstructure of the samples was characterized using a JEOL 7800F field emission gun scanning electron microscope (SEM) and a JEOL 2100F transmission electron microscope (TEM) equipped with an energy dispersive X-ray spectroscopy (EDS) detector. The samples for SEM observations were polished according to standard metallographic techniques and then etched in a hybrid solution (H_2O:HNO_3:HF = 9:9:2). The distribution information of SPPs' size was acquired by the Image-Pro Plus 6.0 software from the SEM image with a magnification of 50000. At least 500 particles from 20 photos of each sample were counted to ensure the reliability of the statistical result. The specimens for TEM observation were prepared using a twin-jet polishing with a mixed solution (C_2H_5OH: $HCLO_4$ = 9:1) at a voltage of 30 V and a temperature of −30 °C. EBSD measurements were carried out with an AZtec HKL Max system, installed on a Mira3 SEM scanning electron microscope.

2.3. Tensile tests

Tensile tests were performed at room temperature with a fixed strain rate of 1×10^{-3}/s using a Zwick Z100/SN3A universal testing machine. Dog-bone flat specimens with a nominal gauge length of 20 mm and a cross section of 12 × 0.6 mm were cut by electric discharge machining from the alloys. The tensile axis was set to be parallel to the rolling direction (RD) and transverse direction (TD). Afterward, the samples were mechanically ground with SiC paper up to 2000 grits.

3. Results

3.1. Mechanical properties

The typical flow curves for the three alloys obtained under the quasi-static tensile tests (10^{-3}/s) are represented in Fig. 2. As is seen, the materials show a relatively higher yield stress when specimens are tested along the TD than along the RD. Such anisotropic response can be explained by the lower Schmidt factor for < a > prismatic slip for tension along TD and by the higher critical resolved shear stresses (CRSS) for the more favorably oriented < c + a > pyramidal glide in the TD [26]. Meanwhile, the trace addition of Cr and V leads to the increment of yield strength of the materials along both directions. A clear yield plateau at the initial stage of yielding is observed in Zir alloy along RD and TD (marked as sky-blue circle in the inset figure). However, this behavior is very weak in Zir-0.1Cr and totally disappears in Zir-0.1Cr-0.05 V alloys. The gradual absence of yield plateau with Cr and V addition at the initial stage of slip deformation is strongly correlated with the microstructures of specimens.

3.2. Microstructure characterizations

The microstructures of samples after the final annealing are characterized by EBSD. Fig. 3 exhibits the inverse pole figure (IPF) maps, grain boundary (GB) maps and mis-orientation angle distribution (MAD) histograms derived from EBSD data for the three alloys. It can be observed from the IPF maps that all the specimens are composed of equiaxed grains, as well as many fine grains among them. However, the orientations (colors) of some grains are not uniform according to the standard triangle at the bottom of Fig. 3. These grains usually have long strip structures along the rolling direction, with non-uniform orientations. It is assumed that the distorted grains are the remnant products

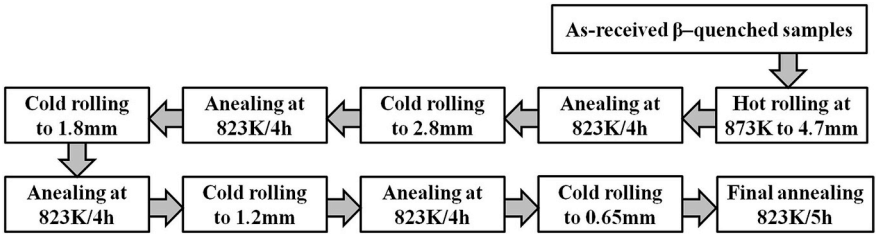

Fig. 1. Schematic of the thermomechanical treatment history of the experimental alloys.

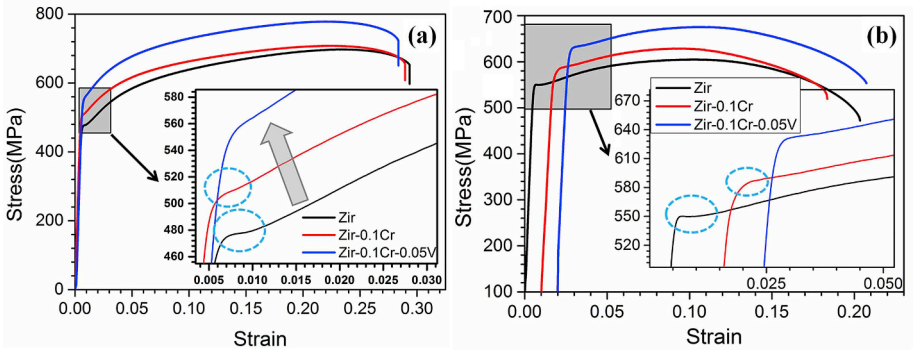

Fig. 2. True stress-strain curves under tension tests for all samples at room temperature: (a) along the RD and (b) along the TD. The inset demonstrates the initial yielding behaviors for three alloys.

by the cold rolling, indicative of the partial re-crystallized microstructures in all the samples after the final annealing. The mean grain size for Zir alloy is 1.9 μm, and this value was decreased to 1.7 μm in Zir-0.1Cr and 1.5 μm in Zir-0.1Cr-0.05 V alloy, respectively. In regard to the GB maps, large amount of low angle grain boundaries (LAGBs, with GB mis-orientations lower than 15°, marked as red line) are dominant in the distorted grains. In general, the sub-grains coalesce together by grain boundaries migration and dislocation slip during the annealing time, resulting in the re-crystallization nucleation behavior. These sub-grains continue to grow up towards the deformed grains, and LAGBs are gradually transformed to high angle grain boundaries (HAGBs, with GB mis-orientations higher than 15°, marked as black line). The MAD maps show that more than half of GBs possess LAGBs for all the samples and the fraction of LAGBs is increased by the addition of Cr and V (from 50.3% to 53.9% for Zir-0.1Cr and 60.8% for Zir-0.1Cr-0.05 V, respectively).

Fig. 4 indicates the typical pole figures of the principle crystallographic orientations in Zir alloy annealed at 823 K for 5 h. It is clear that the basal [0001] direction was preferentially tilted by about 30° from the normal direction (ND) towards transverse direction (TD), and the $[11\bar{2}0]$ and $[10\bar{1}0]$ directions were tend to align with RD. This so-called bimodal basal texture is commonly observed in zirconium, and widely reported by other investigators [27,28]. In general, the texture component of $\{0001\} < 10\bar{1}0 >$ is formed after cold rolling due to the low c/a ratio of Zr (1.589) and the limited number of slip systems [29,30]. During annealing, the basal planes will undergo a rotation by ± 30° around their pole, resulting in the $[11\bar{2}0]$ directions points parallel to RD. This pronounced bimodal basal texture will result in the anisotropic mechanical response of the materials along RD and TD because of the preferential alignment of basal planes in RD. The dislocation slip is highly restricted when samples are loaded parallel to the TD, whereas slip are more easily accommodated in samples along RD, since the prismatic < a > slip system of Zr will be more favorably inclined to the tensile axis [29].

3.3. Precipitate morphology, size and distribution

In the annealing process, some of the alloying elements precipitate as second phase particles (SPPs) to minimize the system energy. Fig. 5 shows the morphology and distribution of the SPPs in the specimens of three alloys. The shape of SPPs is sphere or ellipsoid, and some of them gather together to form clusters. The addition of Cr and V results in a marked increase in the volume fraction of SPPs (Fig. 5b and c). Meanwhile, more clusters are formed by the gathering of SPPs. The size distribution and volume fraction of SPPs measured by SEM images are summarized in Table 2. The mean size is reduced from 72 nm to 57 nm with the addition of Cr and to 60 nm with the combined addition of Cr and V. The volume fraction of SPPs increases from 7.2% to 11.1% and 11.8% in the Cr-containing and Cr + V-containing alloys, respectively.

Fig. 6 shows the bright field TEM micrographs of the specimens, combined with the selected area electron diffraction (SAED) results and EDS results of the analyzed SPPs (marked by white arrows). As shown in Fig. 6a–c, the SPPs exhibit a random dispersion in all the samples, and most of the SPPs situate in the interior of the equiaxed grains. More than twenty particles are analyzed by EDS and SAED in each sample. The EDS spectrums show that the detailed chemical composition (in wt. %) of SPPs is (40.2–45.5)Zr-(27.3–32.6)Nb-(15.5–18.3)Fe-(4.1–10.2)Mo-(0–7.5)Cr-(0–3.8)V in our alloys. The SAED patterns identify that the SPPs in all the samples can be classified into two groups: one with FCC crystal structure, the other with HCP crystal structure. Therefore, it could be concluded that the trace addition of Cr and V could change the chemical composition, but has no effect on the crystal structure of SPPs.

4. Discussion

4.1. Microstructural evolution with the addition of Cr and V

Based on previous microstructural characterization, it can be concluded that trace Cr and V addition into Zir alloy brings some changes on its microstructure, namely reduces the matrix grain size and increases the density of SPPs. The mean grain size reduces from 1.9 μm to 1.7 μm with 0.1% Cr addition, and further reduces to 1.5 μm by the combined addition of 0.1%Cr + 0.05%V. Meanwhile, the fraction of LAGBs gradually increases by the addition of Cr and V, implying that the re-crystallization degree is gradually decreased by Cr and V. It has been well documented that the solute atoms in Zr matrix will decrease the boundary mobility and hinder the boundary moving during re-crystallization [31], which is called dragging effect. This behavior has been reported in zirconium alloys by doping of Mo [32] and Nb [33] and the grain size is gradually reduced with the increment of Mo and Nb contents. Therefore, it is likely possible that the dragging effect of Cr and V into Zir alloys will reduce the grain size and retard the re-crystallization process.

On the other hand, with respect to the famous Zener pinning effect [34] of the SPPs, it has been experimentally demonstrated that in zirconium alloys [35,36], the dislocation motion can be restrained by the SPPs. As displayed in Fig. 4 and Table 2, the volume fraction of SPPs increases from 7.2% to 11.1% with doping of 0.1%Cr, and further increases to 11.8% with doping of 0.1%Cr + 0.05%V. The increment of SPPs' amount can be attributed to the low solid solubility of Cr and V in α-Zr. As reported by Wadman et al. [37], the terminal solid solubility of Cr in α-Zr is only about 70 ppm for zirconium alloy. Using the 3D-APT, Thuvander et al. [38] found that the terminal solid solubility of Cr is 50 ppm in α phase of Zr-2 alloy. Also the solid solubility of V is extremely low [39]. The remnant Cr and V will aggregate in the SPPs and promote the precipitation of the SPPs. As a consequence, an enhanced pinning

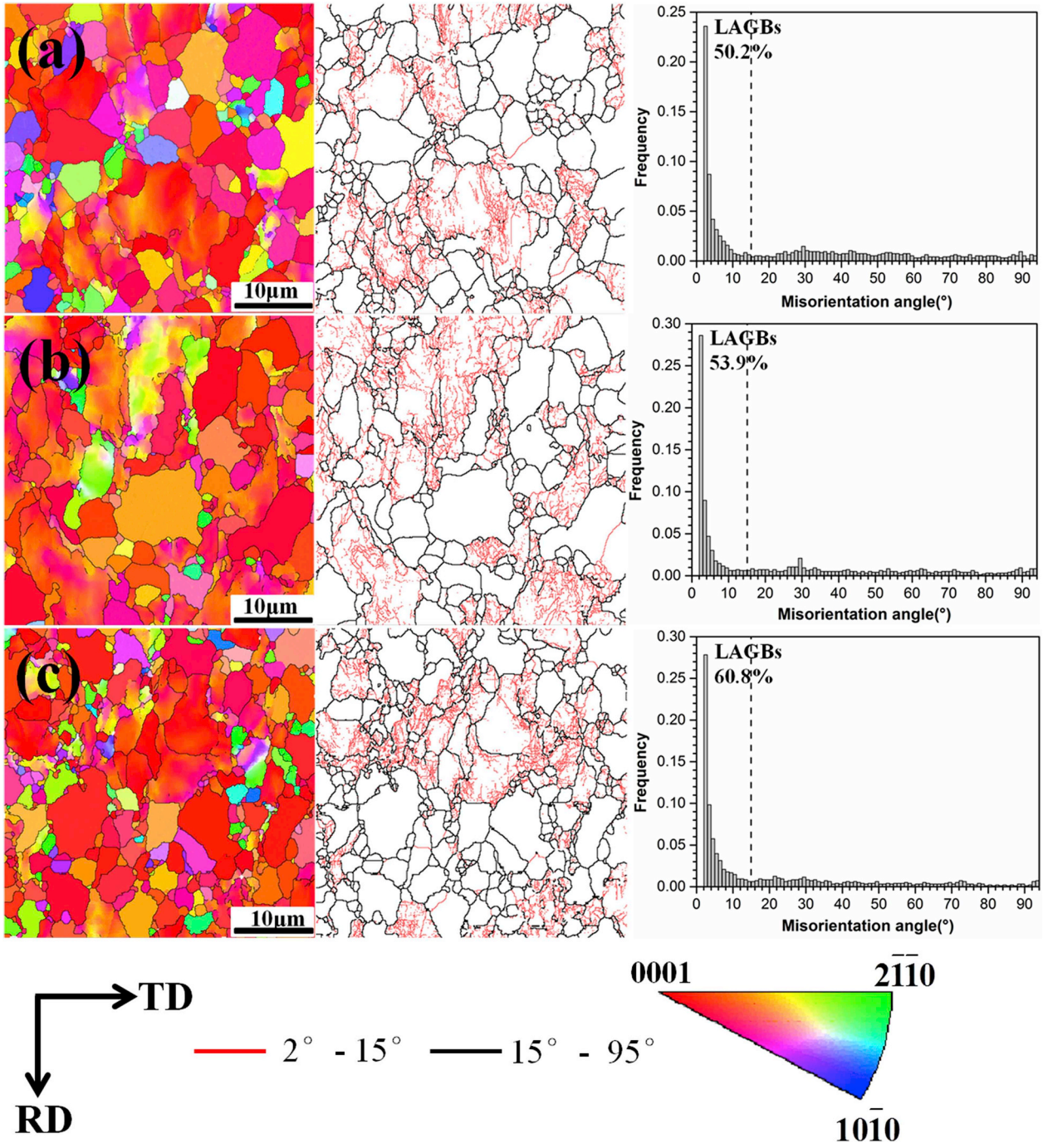

Fig. 3. EBSD inverse pole figure (IPF) map, grain boundary (GB) map and mis-orientation angle distribution (MAD) in the samples of (a) Zir; (b) Zir-0.1Cr and (c) Zir-0.1Cr-0.05 V, respectively.

effect against grain boundaries can be obtained with Cr and V addition in our alloy.

In conclusion, the dragging effect of solute atoms and pinning effect of SPPs are enhanced by the Cr and V addition. This enhancement will reduce the degree of re-crystallization in zirconium alloys, annealed at 823 K, thus leading to the increment of LAGBs and the reduction of grain size.

4.2. Origin for yield point phenomenon and its correlation with microstructure

The most prominent feature in the stress-strain curves is the occurrence of yield plateau in our alloys. A clear discontinuous yielding with yield plateau is observed in the tension tests for Zir alloy, while this phenomenon is very weak in Zir-0.1Cr alloy and totally disappears in Zir-0.1Cr-0.05 V alloy. In general, the presence of yield plateau on the tensile curves can be explained by the dislocation pinning effect, which assumes that the interaction between dislocations and solute atoms facilitates the formation of Cottrell atmosphere [20] or Snoek atmosphere [40]. The classical theory of Cottrell atmosphere is produced by long-range diffusion of solute atoms to edge dislocation line [20]. According to the interpretation of the Snoek-effect [41], the local atomic rearrangement by a short-range diffusion of solute atoms may take place in the stress field of moving screw dislocations. Previous studies [22,23,42] suggested that Snoek pinning of dislocations by paired defects was responsible for the discontinuous yielding in

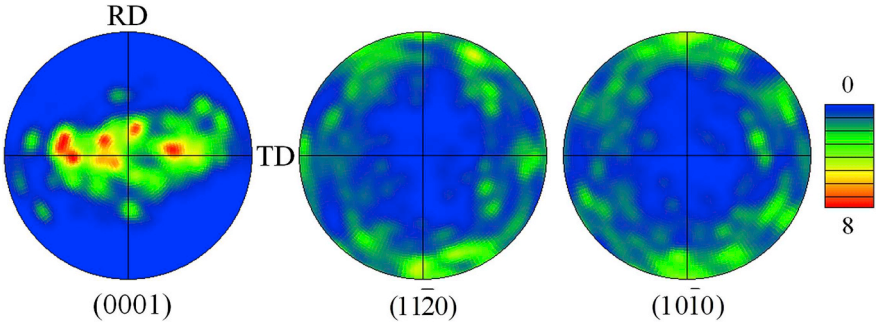

Fig. 4. (0001), (11$\bar{2}$0) and (10$\bar{1}$0) pole figures of Zir alloy annealed at 823 K/5 h.

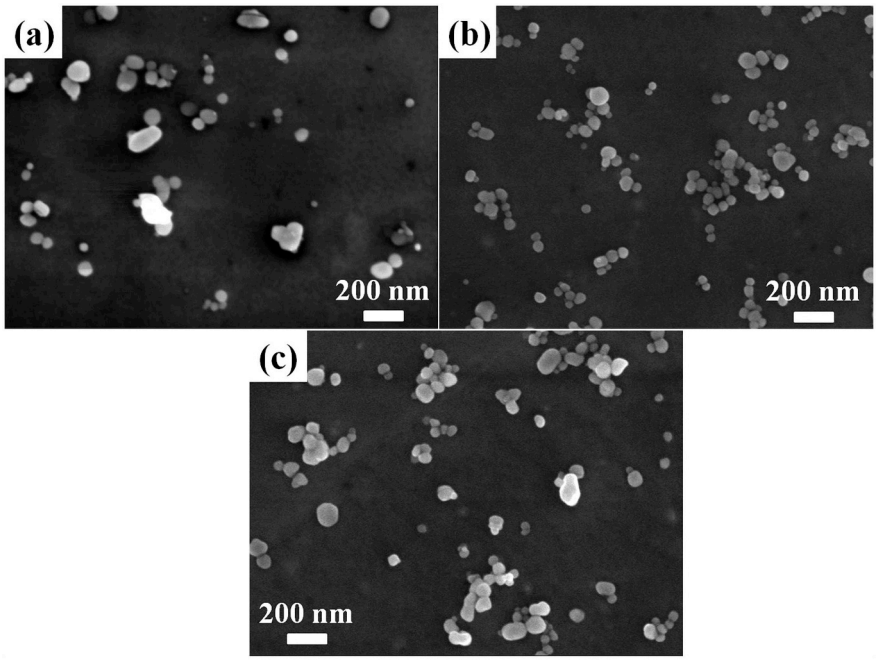

Fig. 5. Morphology and distribution of SPPs in the samples: (a) Zir, (b) Zir-0.1Cr and (c) Zir-0.1Cr-0.05 V.

Table 2
Summary of the microstructural parameters (*d*: mean size of SPPs; *f*: volume fraction of SPPs; *D*: mean grain size of matrix).

Alloy	*d* (nm)	*f* (%)	*D* (μm)
Zir	72	7.2	1.9
Zir-0.1Cr	57	11.1	1.7
Zir-0.1Cr-0.05 V	60	11.8	1.5

zirconium alloys. Veevers [22] concluded that the oxygen-oxygen pairs were responsible for strain aging in irradiated Zircaloy-2. Thorpe and Smith [23] assumed that the Snoek ordering mechanism was responsible for the yield drop in Zr–1Nb alloy. Steuwar [42] found some evidence of stress-induced hydrogen ordering in zirconium hydrides by in situ uniaxial tension tests on hydrided Zircaloy-2 and Zircaloy-4 samples using energy-dispersive synchrotron X-ray diffraction. Therefore, it is likely that the Snoek ordering of interstitial atoms of oxygen may take place in the stress field of dislocations, leading to the dragging effect to some mobile dislocations in our materials. The yield plateau in part can possibly be interpreted by the pinning effect of diffusing oxygen atoms concentrating on < c + a > dislocation arrays gliding on pyramidal planes.

The yield plateau can also be explained in terms of dislocation multiplication mechanism, which was reported by Johnston and Gilman [43]. In their theory, the occurrence of yield drop is correlated with a rapid multiplication of dislocations at the onset of plastic deformation using the following Orowan equation:

$$\dot{\varepsilon} = \rho_m b v \tag{1}$$

and

$$v = v_0 \left(\frac{\sigma}{\sigma_0}\right)^m \tag{2}$$

where $\dot{\varepsilon}$ is the strain rate of materials, ρ_m is the mobile dislocation density, b is the Burgers vector, v is the average velocity of dislocations, v_0 is the unit velocity of dislocations, τ_0 is the stress required for dislocation to move at unit velocity, σ is the effective shear stress acting on the dislocation and m is the stress sensitivity index. When the mobile dislocation density is extremely low, the dislocation velocity must be high in order to maintain the constant value of $\dot{\varepsilon}$., which will lead to the increment of σ and this corresponds to the upper yield point. Once the plastic deformation begins, it will result in the rapid proliferation of mobile dislocations. Thus, the flow stress drops abruptly at the onset of slip deformation, corresponding to the lower yield point.

In Zir alloy, a partial re-crystallized structure is obtained: some deformed grains exist in matrix with non-uniform orientations because of the insufficient final annealing time, and the fraction of LAGBs is

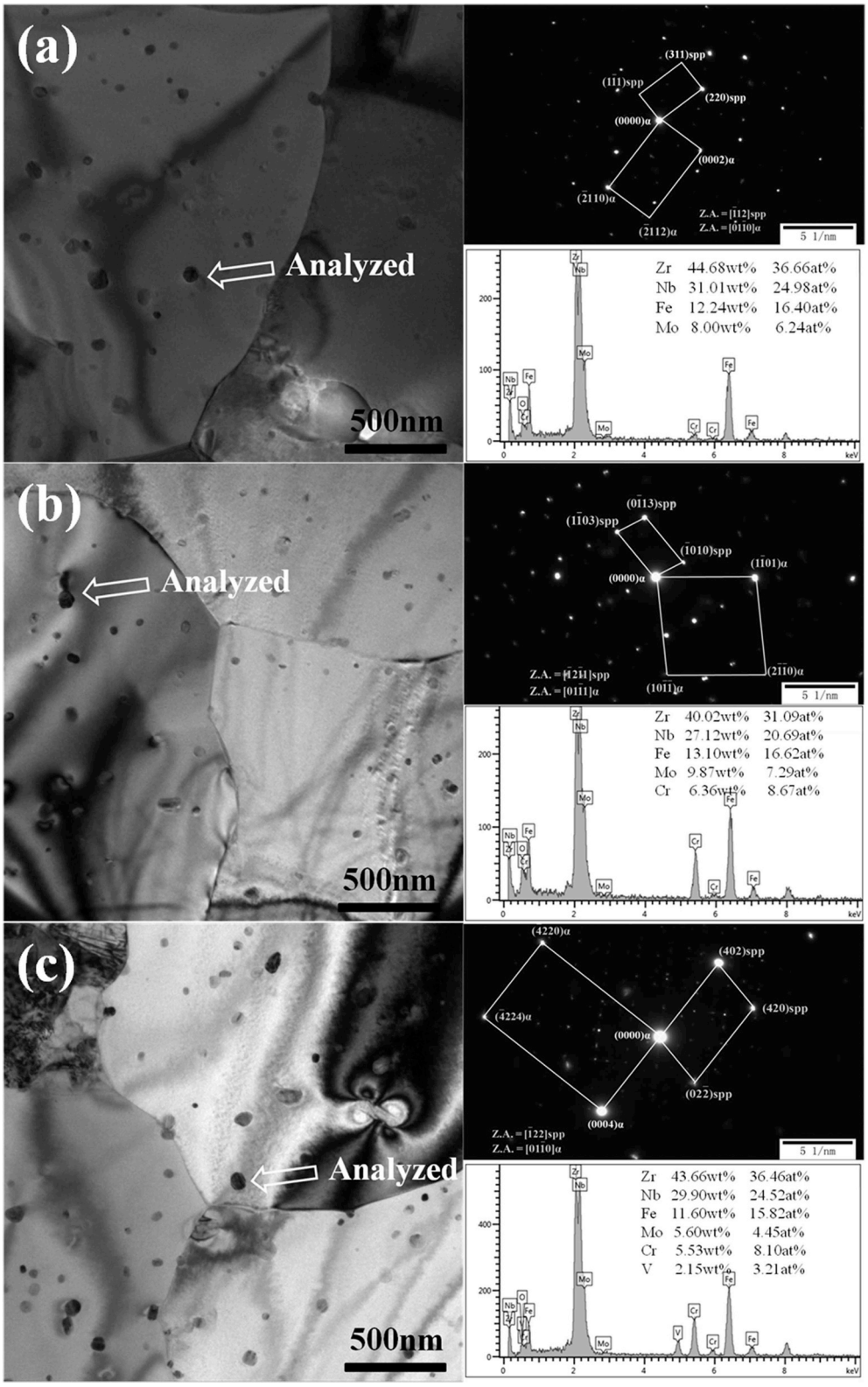

Fig. 6. Typical TEM bright field image, selected area electron diffraction and EDS spectrum with the analyzed chemical composition for (a) Zir, (b) Zir-0.1Cr and (c) Zir-0.1Cr-0.05 V, respectively.

50.3% (Fig. 3a). It is well known that the LAGBs can be considered as a series of edge dislocations, screw dislocations or mixed dislocations, which are arranged parallel or entangled with each other. Fig. 7 shows the typical TEM micrograph of a partial re-crystallized grain in Zir alloy. It is obvious that a large number of dislocations intersect or arrange parallel in the grain interior, corresponding to the large fraction of LAGBs in Fig. 3a. The grain is almost subdivided into several parts separated by dislocations tangling or intersecting, which are the

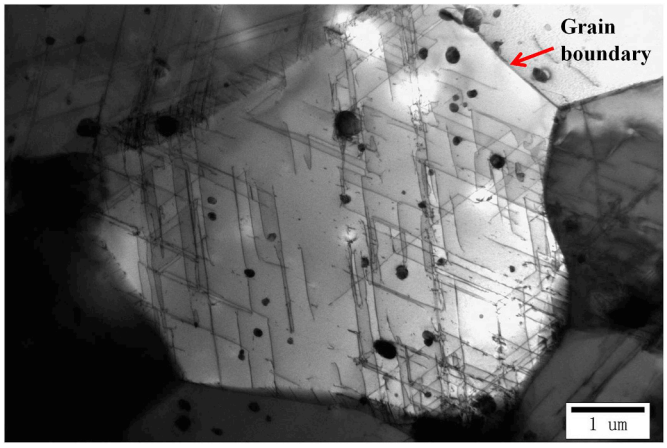

Fig. 7. TEM micrograph of a partially re-crystallized grain in Zir alloy after final annealed 823 K/5 h. Remnant dislocations are still present in the grain after the final treatment.

remnant product of dislocation slip during cold rolling. This high-density dislocation storage will be activated during the initial plastic deformation and most of the dislocations with $< a > = 1/3 < 1\bar{2}10 >$ Burgers vectors lying along pure screw orientations will glide in $(10\bar{1}0)$ prism planes [44,45]. The more LAGBs are, the higher dislocation density is. At the onset of slip deformation, the mobile dislocation density ρ_m is not low in Zir alloy, so the shear stress σ is not high according to equations (1) and (2). After yielding, the mobile dislocation density varies little because the pre-stored mobile dislocations can be activated at the beginning of tensile loading, result in a minor change on the shear stress. Thus, a yield plateau is formed at the early stage of yielding in Zir alloy. With the increase of LAGBs' fraction, the initial density of mobile dislocations increases in Zir-0.1Cr and Zir-0.1Cr-0.05 V. The yield plateau gradually fades away due to the inverse relationship between shear stress and dislocation density. Meanwhile, the redundant dislocations in Zir-0.1Cr and Zir-0.1Cr-0.05 V alloys will interact with grain boundaries and SPPs to enhance the mechanical strength of material. Consequently, higher yield stresses are obtained in Zir-0.1Cr and Zir-0.1Cr-0.05 V alloys, and the yield plateau is replaced by the direct work hardening at the early stage of slip deformation.

In order to validate our inference, tensile tests are performed by modulating the pre-strain history for Zir alloy. Fig. 8 shows the true stress-strain curves obtained by the tensile tests with different pre-strains. When the pre-strain $\varepsilon = 0.5\%$, the stress-strain curve displays a clear yield plateau, indicating that the pre-load deformation has not yet entered the plastic region. The mobile dislocation density has not increased compared with the no pre-strain sample. As the pre-strain increases to 0.6%, a weak yield plateau is observed in the stress-strain curve. With the further increase of pre-strain to 0.8% and 1%, the yield plateau completely disappears, and the larger the pre-strain, the higher the yield strength. It is believed that the pre-strain deformation can introduce a large number of mobile dislocations, and the mobile dislocations increased with increasing pre-strain. As a consequence, the yield plateau gradually disappears with the increase of pre-existed mobile dislocations.

5. Conclusions

Tensile tests were carried out on Zr–Sn–Nb–Fe–Mo alloy with trace addition of Cr and combined Cr and V along RD and TD. A clear yield plateau was observed at the early stage of plastic deformation in Zir alloy along both directions, while this behavior gradually disappeared by the addition of Cr and V to Zir alloy. Microscopic characterization revealed that a partial re-crystallized structure was obtained in each alloy. The addition of Cr and V decreased the degree of re-crystallization and increased the volume fraction of second phase particles (SPPs) in Zir alloy. The enhancement of dragging effect of Cr and V and the pinning effect of SPPs were responsible for the retardation of re-crystallization process. The mechanism underlying the yield plateau in Zir alloy was interpreted by the impurity-dislocation interaction and dislocation multiplication mechanism. The mobile dislocation density varied little at the onset of slip deformation in Zir alloy due to the pre-existing dislocations, leading to a yield plateau as the strain rate was proportional to both the mobile dislocation density and the dislocation velocity. The gradual disappearance of yield plateau was attributed to the gradual increment of mobile dislocation density by Cr and V addition, and the extra dislocations interacted with grain boundaries and SPPs to improve strength of materials. The gradual disappearance of yield plateau can also be reproduced by modulating the pre-strain history in the tensile tests.

Data availability

The raw data required to reproduce these findings are available upon request by email to the corresponding author: luweijie@sjtu.edu.cn.

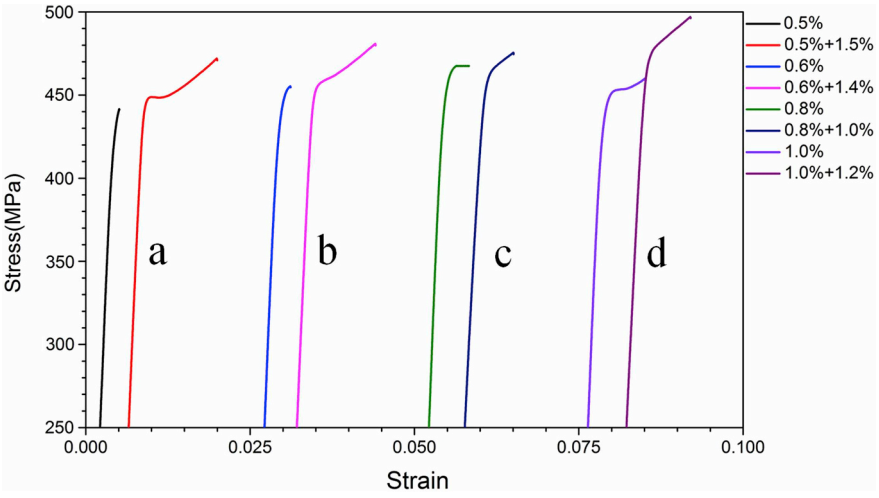

Fig. 8. True stress-strain curves obtained by the tensile tests with different pre-strains for Zir alloy: (a) 0.5%; (b) 0.6%; (c) 0.8%; (d) 1.0%.

Acknowledgements

The authors are grateful to the financial support of the National Natural Science Foundation of China (Grant No: U1602274, 51741108, 51371114, 51875349, 51501112), the 111 Project (Grant No. B16032) and the Laboratory Innovative Research Program of Shanghai Jiao Tong University (Grant No. 17SJ-14).

References

[1] A. Garner, A. Gholinia, P. Frankel, M. Gass, I. MacLaren, M. Preuss, The microstructure and microtexture of zirconium oxide films studied by transmission electron backscatter diffraction and automated crystal orientation mapping with transmission electron microscopy, Acta Mater. 80 (2014) 159–171.
[2] A.T. Motta, A. Couet, R.J. Comstock, Corrosion of zirconium alloys used for nuclear fuel cladding, Annu. Rev. Mater. Res. 45 (2015) 311–343.
[3] A.T. Motta, Waterside corrosion in zirconium alloys, JOM 63 (2011) 59–63.
[4] A. Harte, M. Griffiths, M. Preuss, The characterization of second phase in the Zr-Nb and Zr-Nb-Sn-Fe alloys: a critical review, J. Nucl. Mater. 505 (2018) 227–239.
[5] C.M. Lee, D.S. Sohn, Enhanced high-temperature oxidation resistance of a zirconium alloy cladding by high-temperature preformed oxide on the cladding, Corros. Sci. 131 (2018) 116–125.
[6] R.V. Kulkarni, K.V.M. Krishna, S. Neogy, D. Srivastava, E. Ramadasan, R.S. Shriwastaw, B.N. Rath, N. Saibaba, S.K. Jha, G.K. Dey, Mechanical properties of Zr-2.5%Nb pressure tube material subjected to heat treatments in $\alpha+\beta$ phase field, J. Nucl. Mater. 451 (2014) 300–312.
[7] H.L. Yang, J.J. Shen, Y. Matsukawa, Y. Satoh, S. Kano, Z.S. Zhao, Y.F. Li, F. Li, H. Abe, Effect of alloying elements (Sn, Nb, Cr, and Mo) on the microstructure and mechanical properties of zirconium alloys, J. Nucl. Sci. Technol. 52 (2015) 1162–1173.
[8] Y.I. Jung, Y.N. Seol, B.K. Choi, J.Y. Park, Y.H. Jeong, Effect of Cr on the creep properties of zirconium alloys, J. Nucl. Mater. 396 (2010) 303–306.
[9] O. Zhou, Q. Yao, J. Sun, D.J. Smith, Effect of V addition on the structure of $ZrCr_2$ Laves phase: a high-resolution transmission electron microscopy study, Phil. Mag. Lett. 86 (2006) 347–354.
[10] D. Akama, N. Nakada, T. Tsuchiyama, S. Takaki, A. Hironaka, Discontinuous yielding induced by the addition of nickel to interstitial-free steel, Scripta Mater. 82 (2014) 13–16.
[11] S. Kang, J.G. Jung, M. Kang, W. Woo, Y.K. Lee, The effects of grain size on yielding, strain hardening, and mechanical twinning in Fe-18Mn-0.6C-1.5Al twinning-induced plasticity steel, Mater. Sci. Eng. A 652 (2016) 212–220.
[12] N. Tsuchida, H. Masuda, Y. Harada, K. Fukaura, Y. Tomota, K. Nagai, Effect of ferrite grain size on tensile deformation behavior of a ferrite-cementite low carbon steel, Mater. Sci. Eng. A 488 (2008) 446–452.
[13] A. Momeni, S.M. Abbasi, M. Morakabati, A. Akhondzadeh, Yield point phenomena in TIMETAL 125 beta Ti alloy, Mater. Sci. Eng. A 643 (2015) 142–148.
[14] M. Rezaee, A. Zerei-Hanzaki, A. Mohamadizadeh, E. Ghasemi, High-temperature flow characterization and microstructural evolution of Ti6242 alloy: yield drop phenomenon, Mater. Sci. Eng. A 673 (2016) 346–354.
[15] Z.M. Li, L.M. Fu, B. Fu, A.D. Shan, Yield point elongation in fine-grained titanium, Mater. Lett. 96 (2013) 1–4.
[16] S.M. Abbasi, M. Morakabati, A.H. Sheikhali, A. Momeni, Hot deformation behavior of beta titanium Ti-13V-11Cr-3Al alloy, Met. Mater. Trans. 45A (2014) 5201–5211.
[17] W. Wen, J.G. Morris, The effect of cold rolling and annealing on the serrated yielding phenomenon of AA5182 aluminum alloy, Mater. Sci. Eng. A 373 (2004) 204–216.
[18] M.R. Barnett, M.D. Nave, A. Ghaderi, Yield point elongation due to twinning in a magnesium alloy, Acta Mater. 60 (2010) 1433–1443.
[19] J. Wang, M.R.G. Ferdowsi, S.R. Kada, C.R. Hutchinson, M.R. Barnett, Influence of precipitation on yield elongation in Mg-Zn alloys, Scripta Mater. 160 (2019) 5–8.
[20] A.H. Cottrell, B.A. Bilby, Dislocation theory of yielding and strain ageing of iron, Proc. Phys. Soc. London, Sect. A 62 (1949) 49–62.
[21] M. Griffiths, A review of microstructure evolution in zirconium alloys during irradiation, J. Nucl. Mater. 159 (1988) 190–218.
[22] K. Veevers, K.U. Snowden, Strain aging of quenched Zircaloy-2, J. Nucl. Mater. 47 (1973) 311–316.
[23] W.R. Thorpe, I.O. Smith, Static strain aging of Zr-1 wt% Nb alloy, J. Nucl. Mater. 80 (1979) 35–42.
[24] J.T. Evans, R.M. Douthwaite, Snoek ordering and rapid strain ageing in iron-nitrogen alloys, Acta Metall. 21 (1973) 49–54.
[25] S. Ko, S.I. Hong, K.T. Kim, Y.H. Jeong, Deformation behavior of cold-rolled and annealed Zr-1.5Nb and Zr-1.5Nb-S alloys, J. Nucl. Mater. 414 (2011) 138–144.
[26] K.L. Murty, I. Charit, Texture development and anisotropic deformation of zircaloys, Prog. Nucl. Energy 48 (2006) 325–359.
[27] L. Jiang, M.T. Pérez-Prado, P.A. Gruber, E. Arzt, O.A. Ruano, M.E. Kassner, Texture, microstructure and mechanical properties of equiaxed ultrafine-grained Zr fabricated by accumulative roll bonding, Acta Mater. 56 (2008) 1228–1242.
[28] K.Y. Zhu, D. Chaubet, B. Bacroix, F. Brisset, A study of recovery and primary recrystallization mechanisms in a Zr-2Hf alloy, Acta Mater. 53 (2005) 5131–5140.
[29] Y.N. Wang, J.C. Huang, Texture analysis in hexagonal materials, Mater. Chem. Phys. 81 (2003) 11–26.
[30] E. Tenckhoff, Review of deformation mechanisms, texture, and mechanical anisotropy in zirconium and zirconium base alloys, Proceeding of the 14th International Symposium on Zirconium in the Nuclear Industry, ASTM STP, 2005, pp. 25–50.
[31] K. Lücke, K. Detert, A quantitative theory of grain-boundary motion and recrystallization in metals in the presence of impurities, Acta Metall. 5 (1957) 628–637.
[32] H.L. Yang, S. Kano, Y. Matsukawa, Y.F. Li, J.J. Shen, Z.S. Zhao, F. Li, Y. Satoh, H. Abe, Study on recrystallization and correlated mechanical properties in Mo-modified Zr-Nb alloys, Mater. Sci. Eng. A 661 (2016) 9–18.
[33] H.L. Yang, Y. Matsukawa, S. Kano, Z.G. Duan, K. Murakami, H. Abe, Investigation on microstructural evolution and hardening mechanism in dilute Zr-Nb binary alloys, J. Nucl. Mater. 481 (2016) 117–124.
[34] T. Nishizawak, I. Ohnuma, K. Ishida, Examination of the zener relationship between grain size and particle dispersion, Mater. Trans. 38 (1997) 950–956.
[35] H.G. Shi, X.L. Guo, J.X. Li, J.W. Mao, J.Q. Lu, W.J. Lu, Variation of microstructural features on the tensile property and corrosion resistance of Zr-Sn-Nb-Fe-Cu alloy, Mater. Char. 151 (2019) 84–95.
[36] Y. Matsukawa, H.L. Yang, K. Saito, Y. Murakami, T. Maruyama, T. Iwai, K. Murakami, Y. Shinohara, T. Kido, T. Toyama, Z. Zhao, Y.F. Li, S. Kano, Y. Satoh, Y. Nagai, H. Abe, The effect of crystallographic mismatch on the obstacle strength of second phase precipitate particles in dispersion strengthening: bcc Nb particles and nanometric Nb clusters embedded in hcp Zr, Acta Mater. 102 (2016) 323–332.
[37] B. Wadman, H.O. Andrén, A.L. Nyström, P. Rudling, H. Pettersson, Microstructural influence on uniform corrosion of Zircaloy nuclear fuel claddings, J. Nucl. Mater. 200 (1993) 207–217.
[38] M. Thuvander, H.O. Andrén, Methods of quantitative matrix analysis of Zircaloy-2, Ultramicroscopy 111 (2011) 711–714.
[39] B. Predel, V-Zr (Vanadium-Zirconium), in: O. Madelung (Ed.), SpringerMaterials-the Landolt-Börnstein Database. < http://www.springermaterials.com > .
[40] G. Schoeck, A. Seeger, The flow stress of iron and its dependence on impurities, Acta Metall. 7 (1959) 469–477.
[41] J.T. Evans, R.M. Douthwaite, Snoek ordering and rapid strain ageing in iron-nitrogen alloys, Acta Metall. 21 (1973) 49–54.
[42] A. Steuwer, J.R. Santisteban, M. Preuss, M.J. Peel, T. Buslaps, M. Harada, Evidence of stress-induced hydrogen ordering in zirconium hydrides, Acta Mater. 57 (2009) 145–152.
[43] W.G. Johnston, J.J. Gilman, Dislocation velocities, dislocation densities, and plastic flow in lithium fluoride crystals, J. Appl. Phys. 30 (1959) 129.
[44] E.J. Rapperport, Room temperature deformation processes in zirconium, Acta Metall. 7 (1959) 254–260.
[45] N. Chaari, D. Rodney, E. Clouet, Oxygen-dislocation interaction in zirconium from first principles, Acta Mater. 132 (2017) 416–424.